ON IMPROVED ACCURACY CHIRP PARAMETER ESTIMATION USING THE DFRFT WITH APPLICATION TO SAR-BASED VIBROMETRY

Satish Mandal, Balu Santhanam, and Majeed M. Hayat

Department of ECE, University of New Mexico
Albuquerque, NM: 87131, Email: smandal/bsanthan@unm.edu

ABSTRACT

The estimation of the frequency and chirp rate of a chirp signal in a noisy environment is a fundamental and well-studied problem in signal processing and communications. Its numerous applications include carrier recovery in a communication system, determination of the object position and speed in radar and sonar systems, and many other. Regardless of the application, poor estimation can lead to inaccurate results.

In this paper, we attempt to quantify the accuracy of the *discrete fractional Fourier transform* (DFRFT) approach. We refine prior work to develop analytical expressions for the chirp rate and center frequency parameters. We further study the extensions of this refined DFRFT approach using zero padding, spectral peak interpolation, and chirp-z-transform based zooming. The performance of the refined estimators is compared versus the *Cramer-Rao lower bound* (CRLB) and shown to asymptotically approach the bound.

This refined DFRFT approach is then applied to *synthetic aperture radar* (SAR) vibrometry data from several vibrating targets and the estimated acceleration information and vibration frequencies are shown to be very close to the corresponding ground-truth accelerometer measurements.

Keywords: discrete Fourier transform, discrete Fractional Fourier transform, peak to parameter mapping, chirp rate estimation, center frequency estimation, synthetic aperture radar, vibration estimation

1. MULTI-ANGLE CENTERED FRFT

Vargas-Rubio and Santhanam [1] discussed the *Multi-Angle Centered DFRFT* (MA-CDFRFT) via a eigenvalue decomposition for the DFRFT matrix as

$$\{\mathbf{A}_\alpha\}_{kn} = \sum_{p=0}^{N-1} v_{kp} v_{np} e^{-\jmath p\alpha}, \tag{1}$$

where v_{kp} is the k^{th} element of the p^{th} eigenvector. Multiplying $\mathbf{A}_\alpha$ by the signal x[n], we obtain

$$\mathbf{X}_\alpha[k] = \sum_{n=0}^{N-1} x[n] \sum_{p=0}^{N-1} v_{kp} v_{np} e^{-\jmath p\alpha}. \tag{2}$$

This research was supported by the United States Department of Energy (Award DE-NA 0002494) and the National Nuclear Security Administration (NA-221)

For the discrete set of angles $\alpha = \alpha_r = \frac{2\pi r}{N}$, $r = 0, 1, ..., N-1$

$$\mathbf{X}_k[r] = \sum_{p=0}^{N-1} z_k[p] \mathbf{W}_N^{pr}, \tag{3}$$

where

$$z_k[p] = v_{kp} \sum_{n=0}^{N-1} x[n] v_{np}. \tag{4}$$

Expressing the transform as a *discrete Fourier trnasform* (DFT) allows us to use a radix-2 FFT algorithm to compute the CDFRFT. The resulting transform $\mathbf{X}_k[r]$ containing the CDFRFT for these discrete angles is called multi-angle DFRFT.

Upon application of the MA-CDFRFT to a linear chirp signal, complex or real, sharp peak in the chirp rate versus center frequency representation is formed [2]. A complex chirp signal forms two spectral peaks, one being the reversed version of other while real signal forms four. A real chirp signal of the form

$$x[n] = A\ \cos(\omega_c n + c_r m^2) + w[n], \tag{5}$$

is used for further calculations where $0 \leq n \leq N-1$, $m = n - \frac{N-1}{2}$, c_r is the chirp rate, ω_o is the center frequency and A is the amplitude of the signal and $w[n]$ is the *additive White Gaussian noise* (AWGN). The value of the parameters used in this paper is $N = 128$, $A = 1$, $c_r = 0.001$, and $\omega_c = \pi/3$.

2. RELATION BETWEEN PEAK AND PARAMETER

Once the peak locations are identified, we can apply the peak-to-parameter mapping to get the parameter estimates. Rubio-Santhanam [1] derived an empirical relation between the chirp parameters and peak location which was modified by Peacock and Santhanam [3] as

$$\hat{c}_r = -\frac{\pi}{N} \cot\left(\frac{k_p \pi}{N}\right)\ ,\ \hat{\omega}_c = \frac{2\pi}{N}\left(r_p - \frac{N-1}{2}\right) \csc\left(\frac{k_p \pi}{N}\right). \tag{6}$$

But Ishwor and Santhanam [2] determined that this mapping does not correctly map the peak locations to the corresponding parameters and modified this mapping expression to correctly map the peak location as

$$\hat{c}_r = -\frac{\pi}{N} \cot\left(\frac{2r_p \pi}{N}\right)\ ,\ \hat{\omega}_c = \frac{2\pi}{N}\left(k_p - \frac{N-1}{2}\right) \csc\left(\frac{2r_p \pi}{N}\right), \tag{7}$$

where $\hat{c}_r$ is the chirp rate, $\hat{\omega}_c$ is the center frequency and (k_p, r_p) is the peak location. However, this estimator does not consider the fact that for an even N, the basis vectors of the *centered DFT* (CDFT)

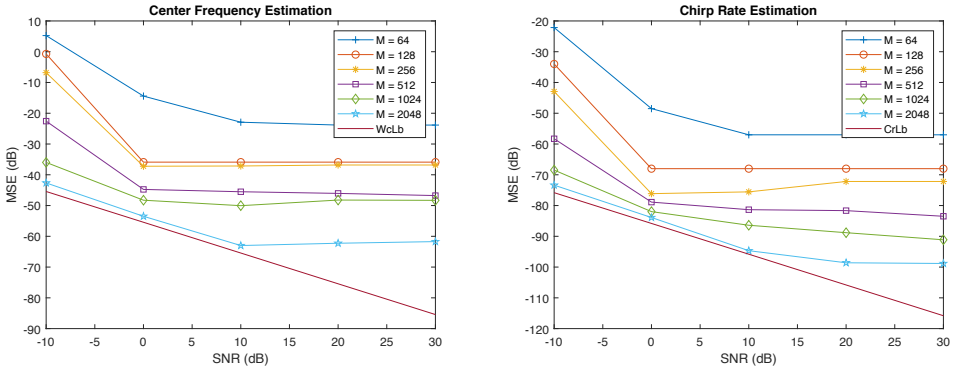

Fig. 1. Performance of the chirp parameter estimators based on the analytical expression and zero padding in DFRFT in comparison to the CRLB, obtained by averaging over 200 experiments.

have a frequency that falls exactly in the middle of the DFT [1]. This means that when computing the CDFT, there is no coefficient for zero frequency, and in some cases this may be an issue. This problem can be solved by shifting the signal to be transformed by a frequency of $\pm\pi/N$. We modified the estimator to incorporate this frequency shift as

$$\hat{c}_r = -\frac{\pi}{N}\cot\left(\frac{2\pi}{N}\left(r_p - \frac{1}{2}\right)\right)$$
$$\hat{\omega}_c = \frac{2\pi}{N}\left(k_p - \frac{N}{2}\right)\csc\left(\frac{2\pi}{N}\left(r_p - \frac{1}{2}\right)\right). \quad (8)$$

3. MA-CDFRFT: ZERO PADDING, SPECTRAL PEAK INTERPOLATION AND CZT ZOOM

3.1. Parameter Estimation via Zero padding

Zero padding is a technique used in spectral analysis for interpolating peaks. It maps the length of signal N to M (where M is larger than N) adding equal amount of zeros at both ends of the signal. Zero padding allows to use a longer CDFT, which in turn produces a longer CDFT result vector. A longer CDFT result has more frequency bins that are more closely spaced in frequency. This results in a smoother looking spectrum. Although it does not improve the resolution of and/or between adjacent nearby frequencies, it makes it easier to visually resolve a single peak at a single isolated frequency that does not have any significant adjacent signals or noise in the spectrum. The analytical expressions are modified to incorporate the zero padding and this is done by replacing N with M.

Fig. (1) depicts the *mean squared error* (MSE) of the center frequency and chirp rate estimates respectively of the zero padding approach as a function of SNR for multiple values of M, $M = 2^6, 2^7, 2^8, 2^9, 2^{10}$, and 2^{11}. We can observe that there is improvement of about 12dB for every quadruple increase in the length of M. So, theoretically, if we kept on increasing the size of CDFT or zero padding over $M = 2048$, the MSE will lie on the CRLB, and we can attain the CRLB asymptotically.

3.2. Parameter Estimation via Spectral Peak Interpolation

This is a two stage method to calculate the parameter estimates using three CDFT samples at the peak. The first stage is to calculated the peak location using the 2D peak estimator. The second stage is to perform a fine search around the peak obtained from the first stage. This method suggests a nonlinear relation involving three samples to a real valued fine resolution of the peak, and thus better chirp parameter estimates.

In the first stage, we calculate the peak locations (r, k). Then, the N-point DFT of the signal is calculated at these points, $A_k = \sum_{n=0}^{N-1} x[n]\, W_N^{nk}$ and $A_r = \sum_{n=0}^{N-1} x[n]\, W_N^{nr}$. Here A_k and A_r denotes the complex valued DFT output. The peak value in the DFT magnitude spectrum (r_p, k_p) is expected to be around the true parameters ω_p and cr_p. Then, we can express the DFT bins where the peak occurs and its immediate left and right neighbors as:

$$A_{k-1} = \sum_{n=0}^{N-1} x[n]\, W_N^{n(k-1)},$$
$$A_k = \sum_{n=0}^{N-1} x[n]\, W_N^{nk},$$
$$A_{k+1} = \sum_{n=0}^{N-1} x[n]\, W_N^{n(k+1)}.$$

Now, we use three different interpolation techniques for fine resolution peak location estimation.

- Parabolic Interpolation [4]:

$$\hat{\delta}_k = \frac{(|A_{k+1}| - |A_{k-1}|)}{(4|A_k| - 2|A_{k-1}| - 2|A_{k+1}|)}. \quad (9)$$

- Candan Interpolation [5]:

$$\hat{\delta}_k = \frac{\tan(\pi/N)}{\pi/N}\,\text{Real}\left\{\frac{(A_{k-1} - A_{k+1})}{(2A_k - A_{k-1} - A_{k+1})}\right\}. \quad (10)$$

- Quinn Interpolation [6]:

$$\alpha_1 = \text{Real}\left(A_{k-1}/A_k\right),\ \alpha_2 = \text{Real}\left(A_{k+1}/A_k\right),$$
$$\delta_1 = \alpha_1/(1-\alpha_1),\ \delta_2 = \alpha_2/(1-\alpha_2),$$
$$\text{if } \delta_1 > 0 \text{ and } \delta_2 > 0,\ \hat{\delta}_k = \delta_2 \text{ else } \hat{\delta}_k = \delta_1. \quad (11)$$

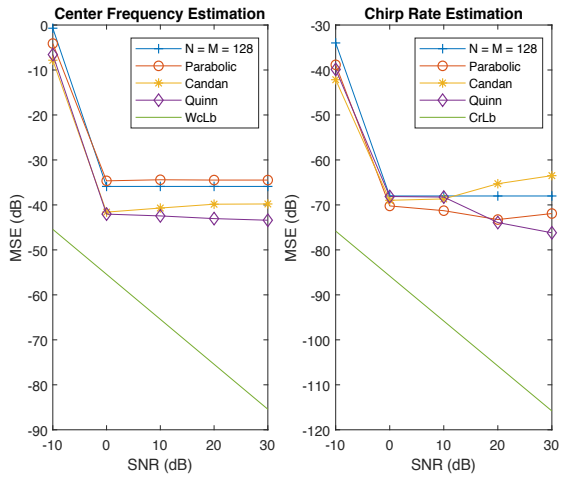

Fig. 2. Effects of interpolation on the chirp parameter estimates.

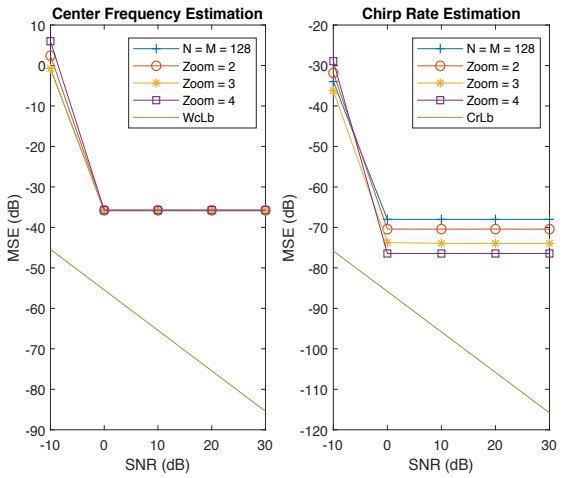

Fig. 3. Effect of CZT-based zoom on the chirp parameter estimates.

The same procedure is repeated for r-index as well. The peak coordinates are then modified as:

$$k_p = k + \hat{\delta}_k \quad \text{and} \quad r_p = r + \hat{\delta}_r \tag{12}$$

Fig. (2) depicts the MSE of both parameters as a result of applying spectral peak interpolation approaches on the peak of the signal. Quinn's Interpolation produces the best results for center frequency estimation, however for the chirp rate, the improvements are minimal.

3.3. Parameter Estimation via CZT Zoom

The CZT-based zoom operation produces zooming in the angle or chirp rate variable r and only affects the chirp rate estimator and not the center frequency estimator. There are two ways to apply the CZT zoom in the MA-CDFRFT algorithm. First, the $(0, 2\pi)$ range of the r-axis is zoomed in to $(0, \alpha * \frac{\pi}{2})$ where $\alpha = 1, 2, 3, ...$ and second, the range is zoomed into the interval $(upperlim, upperlim + \pi/2)$. Here, $upperlim$ is dependent on the zooming factor by,

$$upperlim = \pi/2 - \pi/zoom$$

where $zoom$ is the factor by which we zoom into the r-axis. In the first case, CZT zooming limits the search in the r-axis, thus decreasing the size of the axis itself which in turn increases the r-index number. In order to incorporate this change, the estimators are modified as:

$$\begin{aligned} \hat{c}_r &= -\frac{\pi}{N} \cot\left(\frac{2\pi}{N * zoom}\left(r_p - \frac{1}{2}\right)\right) \\ \hat{\omega}_c &= \frac{2\pi}{N}\left(k_p - \frac{N}{2}\right) \csc\left(\frac{2\pi}{N * zoom}\left(r_p - \frac{1}{2}\right)\right). \end{aligned} \tag{13}$$

While in the second case, the starting point of the r-axis is no longer zero, we have to scale back the peak locations to the $(0, 2\pi)$ range and use the analytical expression to calculate the parameters. If the peak locations after the CZT zoom is (r, k) then Eq. (8) can be used after scaling back the locations by,

$$r_p = 1 + \frac{upperlim + (r-1) * \frac{2\pi}{N * zoom}}{2\pi/N} \quad \text{and} \quad k_p = k$$

In this paper, we employ the first CZT zoom method. This cannot be employed beyond 4-times zoom using this method, however, the second method allows us to zoom beyond that as well. Fig. (3) shows the results of applying CZT-based zoom on the MSE associated with the chirp parameters. We can observe that the improvement is primarily associated with the chirp rate but not the center frequency. There is a consistent improvement obtained by increasing the zooming factor in the MSE of the chirp rate estimates.

3.4. Combination of the Refinements

We observed improvement in the MSE plot for all three refinement approaches. Ideally, combining all the three techniques to form a joint refinement technique would result in better estimate compared to applying single one of the approach. So, we experiment with different combinations of these refinement techniques.

The combination of zero padding with other refinements is studied. We used the zero padded length of $M = 512$, Quinn's interpolation technique and a CZT zoom factor of 2. Again, necessary adjustment to the expressions is made to incorporate these refinements. Figure presents the effect of combining these refinements techniques. Fig. (4) shows the MSE plots for this combination. We can observe that there is a vast improvement in terms of MSE for center frequency parameter using the combination of all three methods. However, the same is not true for chirp rate, which produces the best MSE results for combination of zero padding and CZT zoom. So, we conclude that the combination of zero padding, Quinn's spectral peak interpolation technique, and CZT zoom results in the best possible estimate for the center frequency. The reason is that this combination yields the lowest MSE when compared with the CRLB. However, for the purposes of chirp rate estimation, the combination of zero padding and CZT zoom gives the lowest MSE.

4. APPLICATION TO REAL SAR DATA

SAR is a ubiquitous remote-imaging technique utilized in many disciplines. It can be used in all-weather environments since SARs are active sensors which provide their own illumination, and they work in the microwave spectrum where electromagnetic attenuation is low.

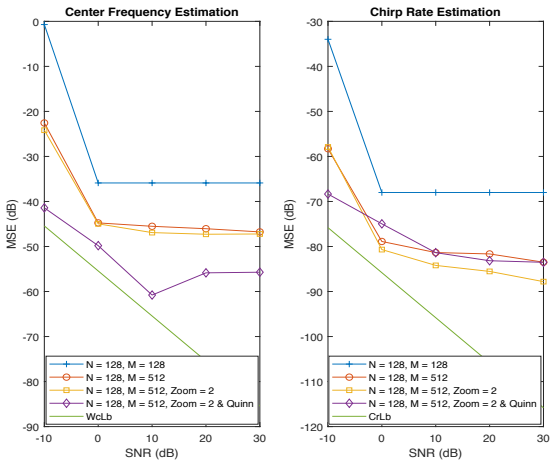

Fig. 4. Effect of zero padding for N = 128 and M = 512 followed by CZT zoom and Quinn's spectral peak interpolation

An underlying assumption when forming a SAR image is that all targets on the ground scene are static. Any vibration movement of targets in the range direction in the ground scene engenders a Doppler shift in the returned SAR signal [8]. This shift causes the vibrating target to manifest as a smearing effect in the SAR images. This smearing manifests itself as a ghost image surrounding the vibrating target at the same range line and results in obscuring the actual target shape [7]. This ghost image creates vibration signatures that help in target identification, retrieve machinery status, and thus detect prohibited activities. In general, these vibration signatures include transient signals like chirped sinusoids, and their associated base frequencies and chirp rate.

4.1. SAR Signal Model

This can be modeled by using a second-order Taylor expansion of the SAR phase-history signal in short-time windows. From [7], this approximation can be stated as

$$x[n] \approx \sigma \exp\left[j\left(\phi - \frac{4\pi f_c}{c} r_d[m] + \left(f_y \bar{y} - \frac{4\pi f_c v_d[m]}{c f_{prf}}\right) n - \frac{2\pi f_c a_d[m]}{c f_{prf}^2} n^2\right)\right] + w[n], \quad (14)$$

where $m \leq n \leq m + N_w$, f_c is the RF carrier frequency, c is the speed of light, f_{prf} is the pulse repetition frequency of the SAR system, $w[n]$ is AWGN, σ is the target reflectivity (constant), $r_d[m]$, $v_d[m]$ and $a_d[m]$ are the instantaneous position, speed and acceleration respectively of the target in the range direction, N_w is the sub-aperture size, $\bar{y}$ is the average azimuth position of the target, f_y is an imaging factor, n is the azimuth bin location, and m is the sub-aperture index.

Using the DFRFT technique and the signal model of Eq. (14), we can estimate the instantaneous acceleration of the vibrating object. In this method, the signal is first approximated by a chirp signal by applying the DFRFT in successive overlapping time windows called sub-apertures. In each of these sub-apertures, we use the analytical expression to calculate the chirp rate from the peak locations. The acceleration of the vibrating target is dependent on the chirp rates estimated at each of the sub-apertures as

$$\hat{a}_d[m] = -\frac{c f_{prf}^2}{2\pi f_c} \hat{c}_r[m], \quad m = 1, 2, 3, .. \quad (15)$$

where $\hat{c}_r$ is the estimated chirp rate at the m-th aperture.

4.2. Description of the Targets

In this paper, we are estimating the vibration signatures and parameters of three types of vibrating targets. Each exhibits a different sinusoidal vibrational behavior. The first is a "top-hat" like chimney reflector, the second target is a rocking quad-corner reflector and the last one is sliding quad-corner reflector. The detailed description about the targets, types of motor, and accelerometer used to study the actual vibration can be found in [9].

The SAR data was collected from a flight test in collaboration with *General Atomics Aeronautical Systems Inc.* (GA-ASI). The data were taken of the targets at 4-in resolution with the Lynx airborne Ku-band SAR system. The system parameters of the Lynx radar for 4-in resolution are detailed in Table 1. The separation between the targets was approximately 100". Figure 5 shows the layout of the target on the ground and its corresponding SAR image at 4-inch resolution.

Table 1. SAR system parameters for the 4-in resolution data.

Parameter	**Quantity**
Pixel dimension	0.0858×0.0885 m^2
Nominal resolution	0.1016×0.1016 m^2
Carrier frequency	$f_c = 15$ GHz
Length of the synthetic aperture	$L = 176$ m
Plane velocity	$V_a = 98$ m/s
Effective pulse repetition frequency	$\hat{f}_{prf} = 185.43$ Hz

4.3. Vibration Estimation

We now apply DFRFT techniques along with the analytical chirp rate estimator in order to distinguish the vibration signatures associated with the three vibrating target. The parameters that are used in the process is shown in Table 2. Here, the sub-aperture (N) is the length of the signal in a moving-window. It is then zero padded to the length M, typically a power of 2, by adding an equal number of zeros on the either side of the signal. While applying the MA-CDFRFT algorithm, we also incorporated a zooming factor of 2. We did not use the spectral peak interpolation technique with this data because as mentioned in previous section, it works best with the estimation of the center frequency but not the chirp rate parameter.

Table 2 also shows the comparison of the acceleration data between the accelerometer measurement attached to the target and the estimated acceleration data using the DFRFT approach. **H.Freq.** and **Amp** denotes the highest frequency component and its amplitude of the acceleration data measured from accelerometer while **E-H.Freq.** and **E-Amp** denotes the highest frequency component and the amplitude of the estimated acceleration data respectively. Note that, this estimated data is obtained from using analytical expression along with refinements. **V-E-H.Freq.** and **V-E-Amp** represents frequency and its amplitude for the estimated acceleration data using just plain vanilla analytical expression. The unit of frequency is Hz while its amplitude is in m/s^2 for all data.

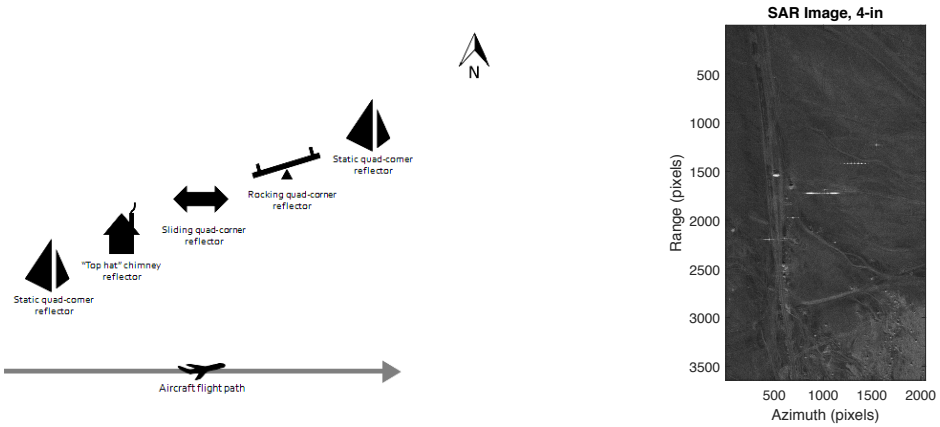

Fig. 5. Layout of the targets in the ground scene and its corresponding SAR image at 4-in resolution.

Table 2. Parameters employed in the DFRFT-based vibrometry technique and comparison between ground truth measurements and estimated measurements.

Target	N	M	Zoom	H. Freq.	Amp	E-H. Freq.	E-Amp	V-E-H. Freq.	V-E.Amp
Top-hat chimney	32	256	2	5.56	0.023	5.07	0.019	0.18/5.07	0.12
Rocking quad-corner	32	256	2	3.43	0.065	3.26	0.070	0.019/3.26	0.07/0.059
Sliding quad-corner	80	256	2	1.29	0.081	1.27	0.084	1.26	0.003

5. CONCLUSION

In this paper, we studied the basics of MA-CDFRFT algorithm and the relation between the chirp parameter estimates using the peak location obtained from the magnitude spectrum of the MA-CDFRFT output. We further modified the existing DFRFT estimator to incorporate a "half-sample" shift. These analytical expressions for the parameter estimates act as an improved version of the empirical estimator. Also combined with various refinements, these expressions produce results that are very close to the CRLB. For the center frequency estimate, the combination of zero padding, spectral peak interpolation, and CZT zoom is optimal while for the chirp rate, the combination of zero padding and CZT zoom is the optimal.

When used in conjunction with SAR-based vibrometry, the instantaneous acceleration calculated from the chirp rate estimated using these expressions is very similar to the acceleration measured with accelerometer. Also, the highest frequency component of the magnitude spectrum of all three vibrating targets is very close to the ground truth. This estimator can be used with cluttered SAR data in conjunction with *Hankel Rank reduction* (HRR) approach described in [10] .

6. REFERENCES

[1] J.G. Vargas-Rubio and B. Santhanam, "On The Multi angle Centered Discrete Fractional Fourier Transform", *IEEE Signal Processing Letters*, Vol. 12, No. 4, April 2005.

[2] Ishwor Bhatta and Balu Santhanam, "A Comparative Study Of Commuting Matrix Approaches For The Discrete Fractional Fourier Transform", *Proc. of IEEE Signal Processing and SP Education Workshop*, pp. 103-108, 2015.

[3] D. J. Peacock and Balu Santhanam, "Multicomponent Subspace Chirp Parameter Estimation Using Discrete Fractional Fourier Analysis," *Proc of IASTED International Conference on Signal and Image Processing*, pp. 326-333, 2011.

[4] M.A. Richards, "Fundamentals of Radar Signal Processing", *New York: McGraw*, 2011.

[5] C. Candan, "A Method for Fine Resolution Frequency Estimation From Three DFT Samples", *IEEE Signal Processing Letters*, Vol. 18, No. 6, June 2011.

[6] B.G. Quinn, "Estimation of Frequency by interpolation using Fourier coefficients", *IEEE Trans. Signal Processing*, Vol. 42, No. 5, pp. 1264-1268, May 1994.

[7] Q. Wang, M. Pepin, R. J. Beach, R. Dunkel, T. Atwood, B. Santhanam, W. Gerstle, A. W. Doerry, and M. M. Hayat, "SAR-based Vibration Estimation using the Discrete Fractional Fourier Transform," *IEEE Trans. Geoscience and Remote Sensing*, Vol. 50, No. 10, pp. 4145-4156, 2012.

[8] R. K. Raney, "Synthetic aperture imaging radar and moving targets," *IEEE Transactions on Aerospace and Electronic Systems* AES-7, pp. 499-505, May 1971.

[9] F. Pérez, J. B. Campbell, M. Jaramillo, R. Dunkel, T. Atwood, A. Doerry, W. H. Gerstle, B. Santhanam, M. M. Hayat, "Exploiting synthetic aperture radar imagery for retrieving vibration signatures of concealed machinery", *Proc. SPIE 9829, Radar Sensor Technology* XX, 982903, 12 May 2016.

[10] F. Pérez, B. Santhanam, R. Dunkel, and M. M. Hayat,"Clutter Suppression via Hankel Rank Reduction for DFrFT-Based Vibrometry Applied to SAR", *IEEE Geoscience and Remote Sensing Letters*, Vol. 14, No. 11, pp. 2052-2056, Nov 2017.